Marine Boundary-Layer Structure and Circulation in the Region of Offshore Redevelopment of a Cyclone during GALE

TEDDY HOLT AND SETHU RAMAN

Department of Marine, Earth and Atmospheric Sciences, North Carolina State University, Raleigh, North Carolina

(Manuscript received 30 March 1989, in final form 28 July 1989)

ABSTRACT

Marine boundary-layer structure and circulation is documented for the 24 February 1986 case of offshore redevelopment of a cyclone during the Genesis of Atlantic Lows Experiment (GALE) Intensive Observing Period (IOP) 9. Mesoscale and satellite information emphasize that the onshore cyclone is not well organized as it moves offshore to the cold shelf waters with redevelopment occurring later over the Gulf Stream region. Within hours of redevelopment, low-level aircraft data were obtained in the region.

Vertical aircraft profiles flown by the National Center for Atmospheric Research (NCAR) King Air in the vicinity of redevelopment over the Gulf Stream, as well as the midshelf front region and cold shelf waters, reveal two distinct boundary layers. Over the Gulf Stream region approximately 50 km south-southwest of the redeveloping cyclone, the near-neutral marine boundary layer ($-h/L = 6.6$) capped by layered stratocumulus is characterized by a low cloud base (360 m), relatively thick stratocumulus cloud layer (800–1200 m) and strong subcloud-layer winds (8–9 m s^{-1}). Associated with the developing cyclone near the Gulf Stream is shallow cyclonic flow with convergence and subsequent acceleration of the wind near the western edge.

Closer to the coast over the cold shelf waters and the midshelf front region, the relatively cloud-free boundary layer ($-h/L = 44.4$) is characterized by a slightly shallower, near-neutral boundary layer ($h = 700$ to 755 m) with very light and variable winds. Boundary layer flow is strongly divergent west of the midshelf front. These two regions are approximately 150–200 km west of the Gulf Stream region of redevelopment.

Flux profiles agree with results from other marine boundary layers under similar cloud and stability conditions and emphasize the warming and moistening of the subcloud layer from near the western edge of the Gulf Stream eastward. Temperature and moisture turbulence structure appear less well organized. The mean momentum budget emphasizes the strong baroclinicity in the MABL and the importance of horizontal advection near the western edge of the Gulf Stream. Comparison of turbulent kinetic energy (TKE) budgets over the Gulf Stream and over the midshelf front show shear production and dissipation to dominate over the Gulf Stream with strong winds. Turbulent transport over the Gulf Stream is a significant term due primarily to the flux of horizontal velocity variance, which is approximately 5 times that of the flux of vertical velocity variance. Over the midshelf front, all normalized terms in the TKE budget are less active in producing, dissipating and transferring TKE for a given heat flux as compared to the Gulf Stream region, where the effects of the developing cyclone are evident.

1. Introduction

The relative importance of the marine atmospheric boundary layer (MABL) in contributing to rapidly or explosively deepening cyclones is not well understood. Even less is known of the boundary layer structure and circulation before such cyclogenesis or in the region of cyclogenesis and how they relate to the intensification or weakening of the cyclone. Several studies have sought to understand the various MABL processes that might contribute to rapid cyclogenesis such as low level baroclinicity, heat and moisture flux exchange from the ocean, latent heat release and static instability (Nuss and Anthes 1987; Bosart and Lin 1984; Gyakum 1983). Such studies, however, have not considered the MABL structure preceding cyclogenesis or in the redevelopment offshore of the cyclone mainly because of the lack of such data from a comprehensive observation network with an emphasis on MABL structure. The case here represents a unique opportunity to study the MABL structure in the region of offshore intensification/redevelopment of a surface cyclone. Data are obtained in the region of redevelopment of an onshore cyclone near the Gulf Stream within hours of redevelopment.

The Genesis of Atlantic Lows Experiment (GALE), conducted from 15 January to 15 March 1986 along the east coast of the United States, was designed to study the factors affecting the development and intensification of East Coast storms (Dirks et al. 1988). The experiment consisted of a vast observation network including radars, ships, buoys, an automated mesoscale network (PAM), radiosondes and a Cross-chain Loran Atmospheric Sounding System (CLASS). The boundary layer subprogram of GALE used the National Center for Atmospheric Research (NCAR) King Air and

Corresponding author address: Dr. Sethu Raman, Department of Marine, Earth and Atmospheric Sciences, Box 8208, Raleigh, NC 27695.

Electra aircraft as primary observation platforms. (See Raman and Riordan 1988, for details on the boundary layer subprogram).

Over 25 boundary layer research flights were flown by the two aircraft during GALE, studying a variety of boundary layer processes. The King Air research flight of 24 February 1986 is considered in this study. The purpose of this paper is to document the structure of the MABL and the associated circulation near the Gulf Stream using the 24 February 1986 case to understand the role of the MABL in offshore redevelopment. Observations will be compared to other boundary layer experiments to help understand differences in boundary layer processes and structure. King Air aircraft data will be the primary dataset, but supporting observations from ships, buoys and PAM and CLASS networks will also be used.

2. Weather synopsis: 24 February 1986

GALE Intensive Observing Period (IOP) 9 was characterized by rapid development and intensification offshore of the surface cyclone that moved through the network on 24 February (Mercer and Kreitzberg 1986). At 12Z 24 February (synoptic times in two digit hours, Z), the National Meteorological Center (NMC) analysis (Fig. 1a) positioned the surface cyclone (1010 mb) in south central Kentucky just west of the Appalachian Mountains with a strong warm front, evident from the PAM network, stretching along the South Carolina–Georgia border. Flow at 850 and 500 mb (Figs. 2a, d) indicated a significant upper level short wave with the trough axis at 500 mb aligned roughly over the surface low with a 1.6×10^{-5} s^{-1} vorticity maximum just west of the trough. Six hours later (18Z)

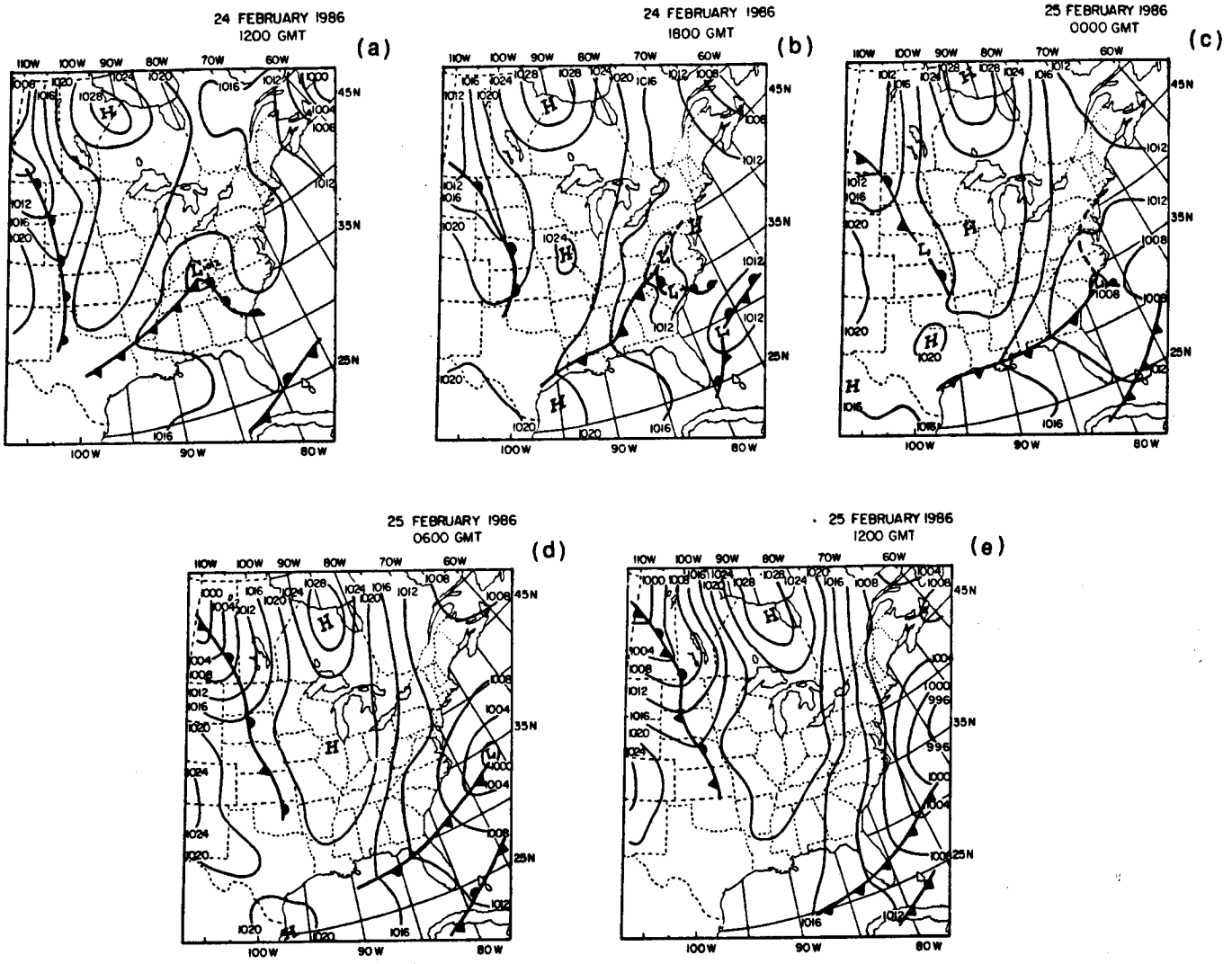

FIG. 1. NMC surface pressure analysis for (a) 1200 UTC 24 February 1986, (b) 1800 UTC 24 February, (c) 0000 UTC 25 February, (d) 0600 UTC 25 February and (e) 1200 UTC 25 February 1986. Isobars are given every 4 mb.

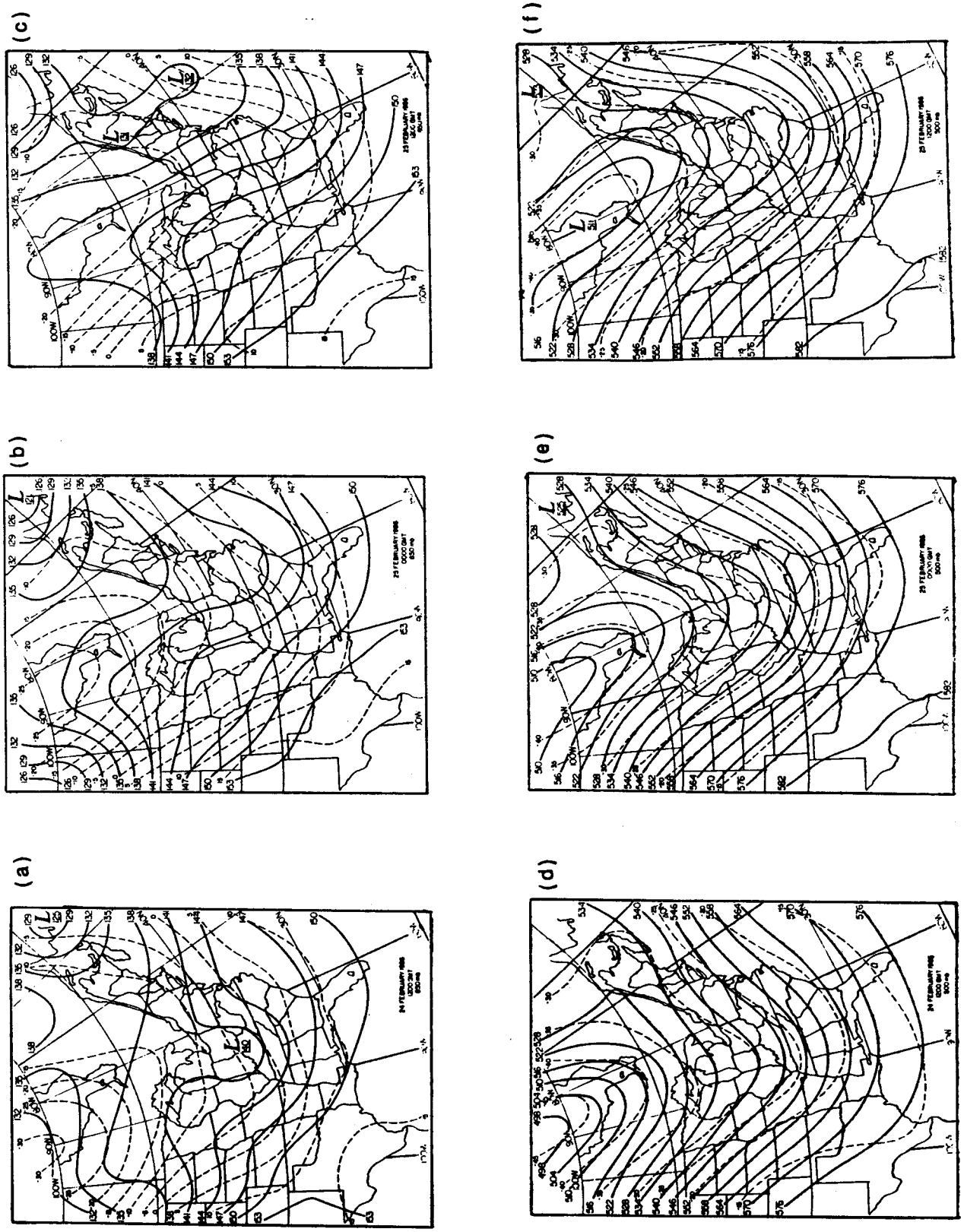

FIG. 2. NMC 850 mb analysis for (a) 1200 UTC 24 February 1986, (b) 0000 UTC 25 February, (c) 0600 UTC 25 February; and 500 mb analysis (d)–(f) for the same time period. Solid lines are isopleths of geopotential in decameters. Dashed lines are temperatures in °C.

(Fig. 1b) upon crossing the Appalachians, the surface cyclone became less defined with a broader region of low pressure east of the mountains. The surface warm front could be identified easier over land than over water having progressed northward to central South Carolina. Over the ocean the progression of the warm front and the offshore movement or redevelopment of the surface low was more difficult to identify.

Mesoscale surface analysis from the PAM network, ships and buoys for 1800–2300 UTC 24 February in the region of the warm front offshore of South Carolina (Fig. 3) indicates the difficulty in pinpointing the front over the ocean. At 18Z (Fig. 3a) moderate northeasterly flow (10 kt) along the coast from Cape Hatteras (35.3°N, 75.5°W) to Wilmington, North Carolina (34.3°N, 77.9°W) contrasts the south-southwesterly flow in the vicinity of Charleston, South Carolina (32.9°N, 80.0°W). The data sparse region (centered near 31°N, 76°–82°W) makes it difficult to determine a frontal boundary. Visible satellite imagery at 18Z (Fig. 4b), however, indicates little organized cloud activity in this region, sugggesting that if a warm front existed at this time, convective activity was weak.

A more interesting feature in the 1600 and 1800 UTC satellite observations is the presence of organized cloud activity centered at 33°N, 76.5°W. Mesoscale analysis and satellite imagery confirm the development of cyclonic rotation from 1900 to 2200 UTC offshore (33°N, 76.5°W), indicating possible redevelopment of the surface cyclone that had moved through the inner GALE network over land. This strong circulation was not evident earlier (12–16Z) west of 33°N, 76.5°W (over the cold shelf water) suggesting that the strong cyclone did not strengthen in the region offshore but redeveloped somewhere near the Gulf Stream in an environment suitable for possible cyclogensis. The 1600 UTC satellite picture (Fig. 4a) appears to confirm this hypothesis, showing cyclonic development near 33°N, 76.5°W. The location of this redevelopment is near the western edge of the Gulf Stream in the region of the NCAR King Air boundary layer flight (see section 3). The flight occurred within about 6 hours of the noticeable redevelopment.

By 00Z 25 February the NMC surface analysis (Fig. 1c) situated the 1007 mb low erroneously at the coast instead of offshore as illustrated by mesoscale and satellite information. It should be noted that there had been little deepening of the low in the previous 12 hours. The axis of the 850 and 500 mb troughs had progressed over central North Carolina (Figs. 2b, e) with a 500 mb vorticity maximum of 1.6×10^{-5} s^{-1} at the North Carolina–South Carolina border just onshore. Six hours later the NMC surface analysis indicated that the surface low had deepened 8 mb to 999 mb and had moved northeast along the western Gulf Stream boundary. By 12Z 25 February (Fig. 2e) the surface low had moved northeast and further deepened (990 mb). The upper level trough progressed eastward over North Carolina with significant cold air advection evident at 850 mb offshore of the Carolinas (Fig. 3c).

By 06Z 26 February the surface low had joined further offshore with the low pressure center associated with the remnant cold front located to the south to form a 973 mb low—a deepening rate of 34 mb in 30 hours. This rapid deepening was not forecast by the numerical models, nor was the offshore redevelopment of the surface cyclone. A variety of factors could be important, most notably the interaction of the boundary layer with the upper levels. The erroneous location of the surface cyclone due to the lack of information in the boundary layer, particularly near the Gulf Stream, along with the underprediction of the amplifying 500 mb short-wave trough could have contributed to the underforecast of the rapid intensification offshore.

3. Aircraft observations

a. Flight plan

The flight track of the NCAR King Air on 24 February offshore of South Carolina is given in Fig. 5 along with the high resolution (2.5 km) sea surface temperature (SST) field obtained from the NOAA-9 satellite. Positions B, D and C indicate regions of vertical profiling as shown in the flight tracks (Fig. 6). The western edge of the Gulf Stream is indicated by GS (Fig. 5). A level-wing descent from 10 000 feet was first flown at B (33.0°N, 79.0°W) over the cold shelf waters (SST = 13°–15°C) to obtain vertical boundary layer structure. The flight proceeded from B at 40 m altitude to C (32.8°N, 76.7°W) located over the Gulf Stream (SST = 24°–25°C) to map low level winds and temperatures. Data from this low level transect are given in Fig. 7. At C a vertical stack consisting of a series of level 230 to 330 second legs (18.4 to 26.4 km in length at an aircraft speed of 80 m s^{-1}) at four altitudes in the subcloud layer was flown. One level flight was also made above cloud top in the free atmosphere.

The flight from C to D (midshelf front) was at approximately 30 m below cloud base (roughly 330 to 380 m). At D (33.0°N, 78.0°W) another vertical stack was flown similar to that at C; however, SST at D in the midshelf region was only approximately 20°C. Upon completion of the last leg at D (1550 m), a level-wing, constant heading (330°) descent was flown from D to E (33.5°N, 78.3°W) to obtain vertical boundary layer structure to the north and east of the low level transect.

The desired orientation of the vertical stacks at C and D in the boundary layer was to align them perpendicular to the mean wind direction. Such an alignment is optimal for the determination of turbulent fluxes (LeMone 1973). It was also desired to fly roughly parallel to SST isotherms to avoid conditions of large

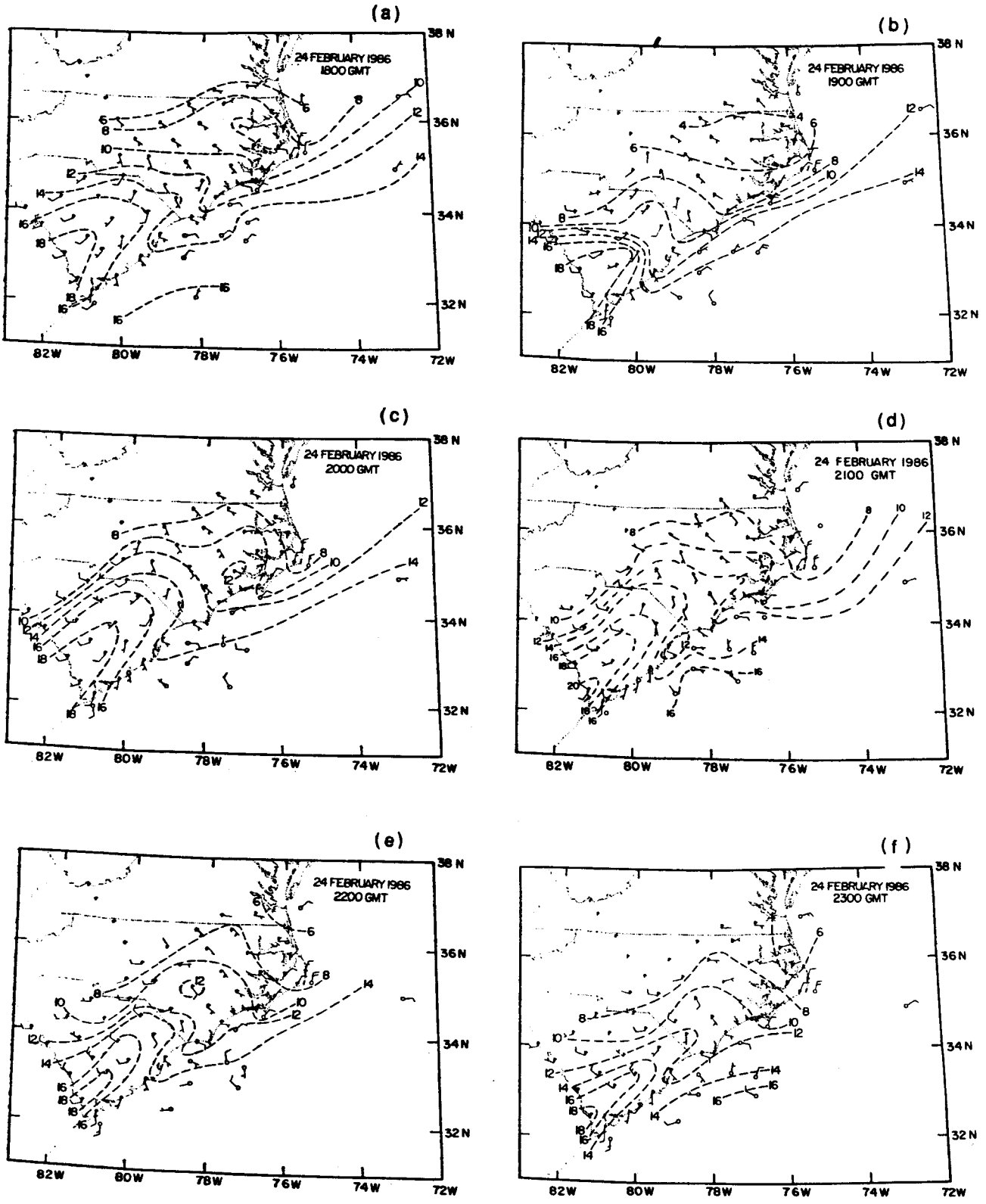

FIG. 3. Mesoscale surface analysis based on available ship, buoy and PAM data in the GALE region for 24 February at (a) 1800 UTC, (b) 1900 UTC, (c) 2000 UTC, (d) 2100 UTC, (e) 2200 UTC and (f) 2300 UTC. Dashed lines are isotherms (°C) and wind barbs are in knots.

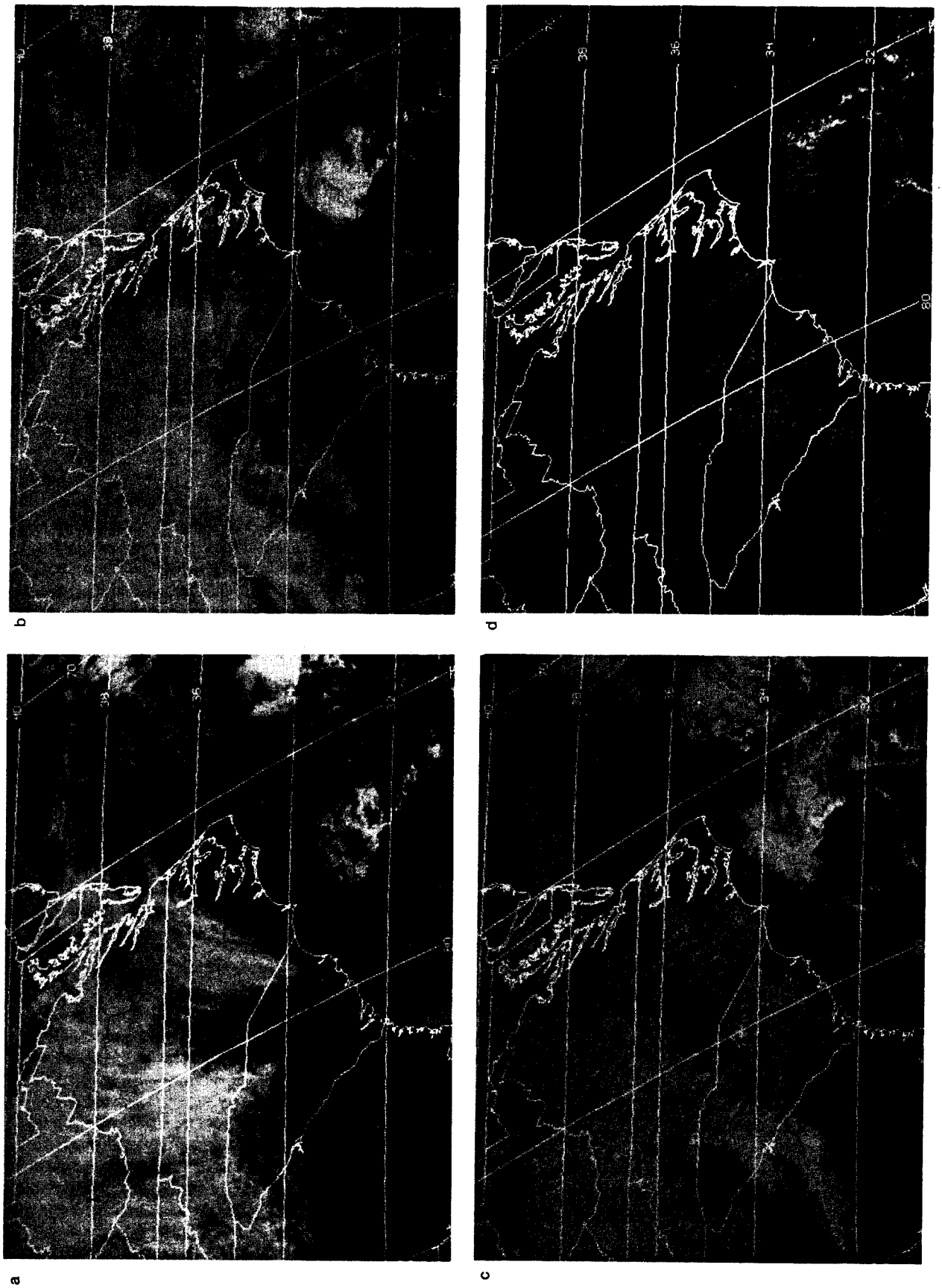

FIG. 4. Visible satellite pictures from GOES-6 for 24 February 1986 at (a) 1600 UTC, (b) 1800 UTC, (c) 2000 UTC and (d) 2200 UTC. The offshore redevelopment of the cyclone is evident near 33°N, 77°W. Also shown is the King Air flight track over the ocean from B-C-D-E from approximately 2000–2300 UTC.

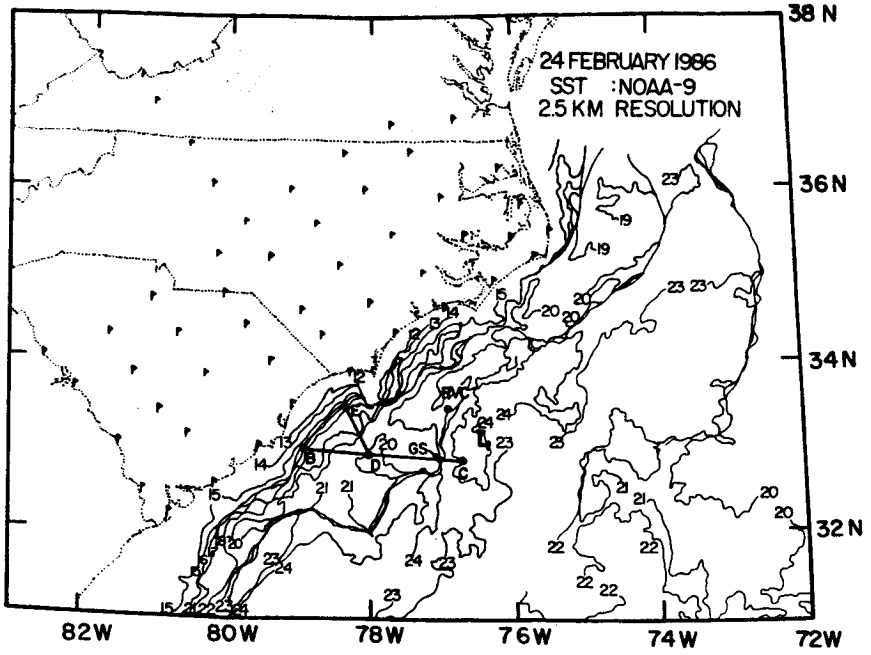

FIG. 5. High resolution sea surface temperature field obtained from NOAA-9 satellite imagery on 24 February. Isotherms are every 1°C. The position of the western edge of the Gulf Stream is indicated by GS and the position of the surface cyclone center by L.

horizontal inhomogeneity. Stack C satisfied both conditions, with the heading of 350° being within 10° of crosswind and little SST gradient to the north (Fig. 5). At stack D surface winds were much lighter and variable. A 350° heading was chosen because of the weak SST gradients to the north; however, this resulted in stack legs aligned more alongwind (within 15°) as opposed to the desired crosswind. Implications of such an alignment on turbulence statistics are discussed in section 5b.

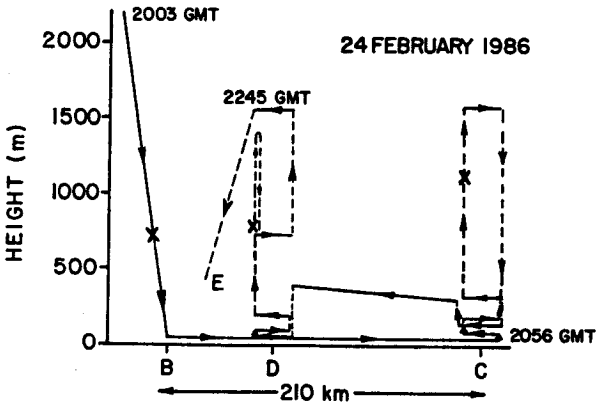

FIG. 6. Vertical profile of the King Air flight track on 24 February. Boundary layer stacks were flown at both C and D. Boundary layer depth h at each location obtained from ascent or descent profiles is indicated by (×).

Satellite pictures at the time of the King Air flight (20–22Z) indicate a lack of clouds and only thin haze at B and D east of the Gulf Stream (Figs. 4c, d). However, deepening stratocumulus clouds are present near the western edge of the Gulf Stream west of C in association with the offshore cyclone.

b. Instrumentation and data

Instrumentation onboard the King Air is similar to that of the Electra discussed in detail by LeMone and Pennell (1980) or Lenschow and Spyers-Duran (1986). Only a brief discussion of the primary mean and turbulence quantities is included here. Both low-rate, 5 samples per second (sps) and high-rate (50 sps) data were obtained from the aircraft instrumentation system. Postflight processing involved first digitally filtering all data using a four-pole low-pass Butterworth filter with a 10 Hz cutoff frequency. High-rate data were then interpolated to 20 sps. Low-rate data were block-averaged over the 5 sps data centered at the start of each second to obtain 1 sps data.

Onboard the aircraft, ambient temperature was measured by a Rosemount temperature probe, dewpoint by an EG&G dewpoint hygrometer and pressure by a Rosemount pressure transducer. A radome gust probe with pressure ports on the nose of the King Air was used for sensing air motion. Both mean horizontal wind and turbulent fluctuations of the three air velocity components were obtained from the radome and the

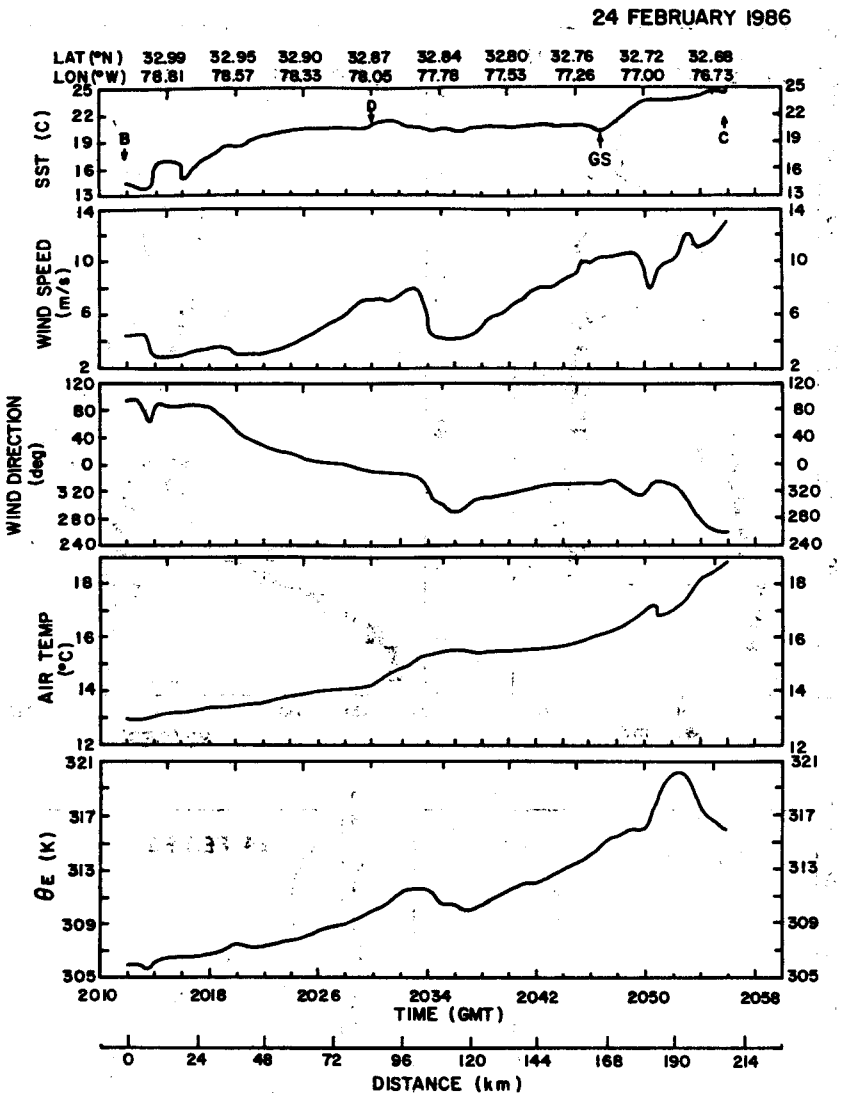

FIG. 7. Data obtained from the King Air low-level (40 m) transect from B to C on 24 February. Data are smoothed by eye. Note the increase in wind speed near C where winds shift to westerly. Stack C was approximately 50 km north-northeast of the surface cyclone.

inertial navigation system (INS). Subtraction of the velocity of the airplane, measured by the INS, from the velocity of the air, obtained from the differential pressure measured across the ports on the radome, yielded the wind components (Brown et al. 1983).

High-rate humidity values were obtained from the Lyman-alpha absorption hygrometer. Reduction of raw voltage output from the Lyman-alpha involved a linear regression on the slow response absolute humidity obtained from the dewpoint hygrometer for 114 one-minute average values similar to the method of Friehe et al. (1986). The correlation coefficient was 0.994.

Mean and turbulence values over the length of each flight leg were then detrended by linear regression. Any spurious spikes, represented by values exceeding three standard deviations, were also removed. Means, standard deviations and fluxes were then computed from detrended data for each leg.

4. Mean boundary layer structure

Figure 8 shows the mean vertical profiles of wind speed (WS) and direction (WD), potential temperature (Θ) and absolute humidity (Q) obtained from King Air data on 24 February. Given are level-wing aircraft descent profiles at B (2005 UTC) and ascent profiles at C (2120 UTC) and D (2228 UTC) along with leg-averaged values at stacks C and D. Dashed horizontal lines indicate the boundary layer height h obtained from the ascent or descent profiles for the three regions (h_B, h_C, h_D). Determination of h from aircraft profiles is difficult particularly when clouds are present (Albrecht et al. 1985; Brost et al. 1982a). The criteria used

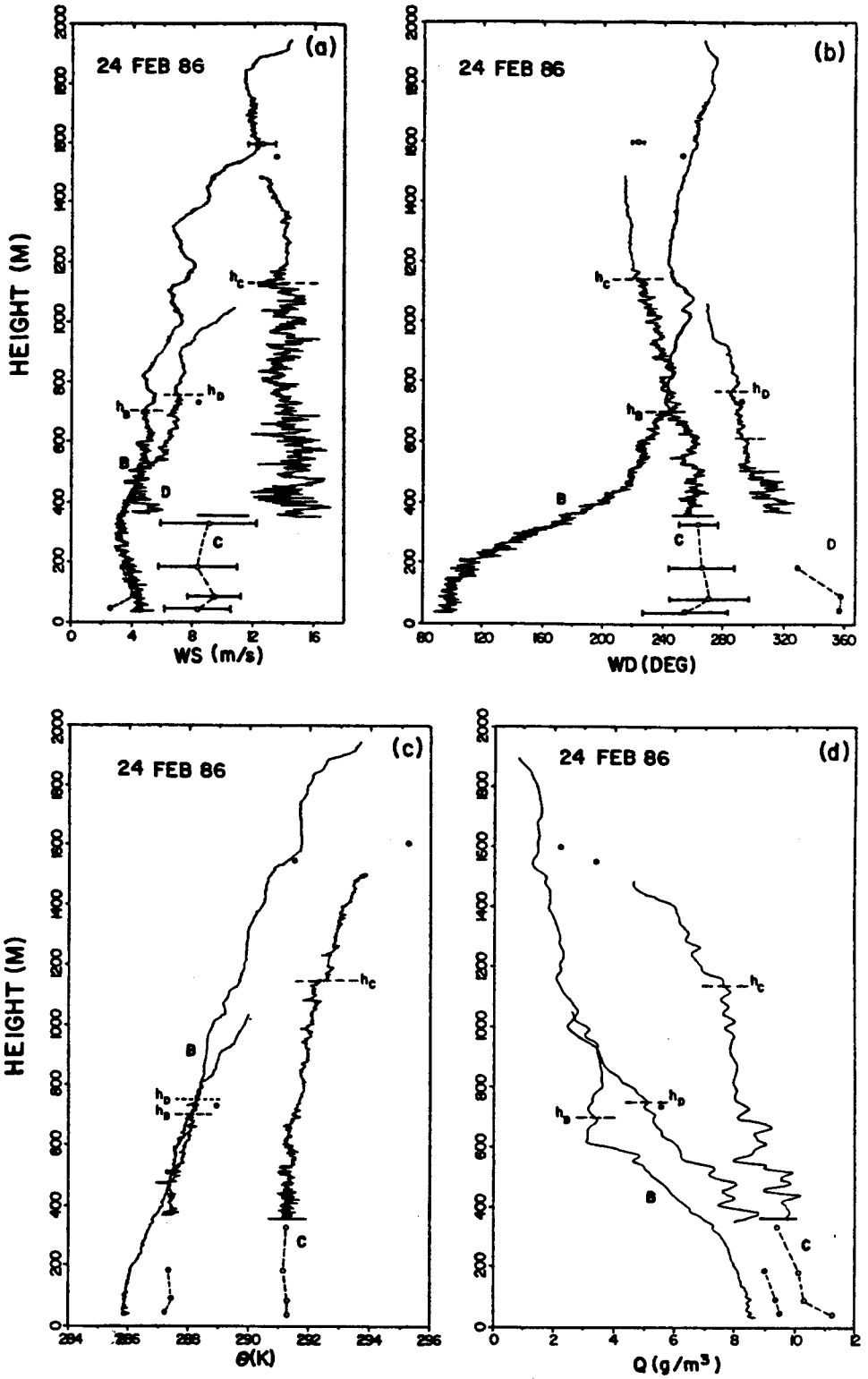

FIG. 8. Mean vertical profiles of (a) wind speed (WS) and (b) direction (WD), (c) potential temperature (Θ) and (d) absolute humidity (Q) obtained from King Air ascent and descent profiles at B, C and D and stack profiles at C (open circles) on 24 February. Dashed horizontal lines indicate boundary layer depth (h_B, h_C, h_D) obtained from the descent profile at B and the ascent profiles at C and D. Cloud base for region C is indicated by the solid horizontal line. For wind speed and direction leg-averaged values at C, ± one standard deviation is also indicated.

here to determine h were: (i) regions where turbulence was significantly damped and/or (ii) regions of sharp gradients (i.e, jumps) in mean profiles, and for the stratocumulus-topped MABL at stack C, (iii) the height of the cloud tops.

For the cloud-free boundary layers at B and D, determination of h was more straightforward than at C. Regions of decreased turbulence at 705 m (B) and 755 m (D) clearly marked the depth of the MABL. Near stack C the presence of layered and scattered stratocumulus made determination of h_C more difficult. In agreement with others (Chou and Zimmerman 1989; Grossman and Betts 1990; Brost et al. 1982a), cloud top is chosen as the depth of the MABL at stack C in contrast to cloud base for shallow, cumulus-topped boundary layers over ocean and land. No transition layer in the Θ profile typically observed for decoupled cloud and subcloud layers is evident at stack C, suggesting a coupling of the overlying stratocumulus deck and the subcloud layer over the Gulf Stream. In fact, the depth of the subcloud layer is observed to shrink and the depth of the cloud layer to thicken eastward over the Gulf Stream to stack C, indicating that the MABL is being warmed and moistened from below, but also that the subcloud layer warming does not compensate for the subsequent moistening.

At stack C, cloud base (360 m) was clearly defined from onboard aircraft observer's reports, but, cloud tops varied from approximately 1140 to 1560 m. Thus, from the aircraft ascent profile at C (Fig. 8) and observer's reports, a boundary layer height of 1140 m is chosen based on the marked decrease in turbulence in the wind components, a small jump in potential temperature (0.5°K) and a noticeable change in the vertical gradient of moisture.

Comparison of temperature and moisture profiles at B, C and D indicates, as expected, a much warmer, moister boundary layer at C over the Gulf Stream. Profiles at B and D are similar—a near-neutral boundary layer with decrease of moisture with height with both B and D roughly 4.5°–5.5°C cooler and 1.5–2.0 g m^{-3} drier than those observed at C. At D (SST = 20°C) vertical temperature and moisture profiles would be expected to be much warmer and moister than observed; however, the northerly low level flow advects cooler, drier air to D as compared to the relatively warmer easterly flow at B. Thermodynamic profiles at C are also not as warm and moist as typically observed for the Gulf Stream region with a SST of approximately 25°C. Mean low level westerly flow advects slightly cooler, drier air, although the winds in the boundary layer near C are variable—shifting markedly with time in association with the redevelopment of the cyclone.

The vertical profiles of wind speed and direction at B, C and D indicate significant differences. Little vertical shear is evident at B (cold shelf waters) up to a height of 1 km with winds approximately constant (4.0–5.5 m s^{-1}); however, there is large directional shear. In the lowest 150 m, the mean flow is easterly (onshore) and thus very shallow. Winds at altitudes as low as 350 m shift to southerly, veering to southwesterly above 600 m. At D light (2–4 m s^{-1}) northerly winds are observed in the lowest 150 m, supported by observations from the low-level aircraft transect (Fig. 7), with little vertical wind shear. Above 200 m winds back to northwesterly. At C (Gulf Stream) in the region of the offshore cyclone, westerly winds in the subcloud layer are observed of twice the magnitude (8–9 m s^{-1}) as at B and D, but with little directional shear. Shown in Fig. 8 for the leg-averaged wind components at C are ±1 standard deviation indicating the variability in the winds at C. The apparent large jump in wind speed at C at the cloud base observed from leg-averaged values to aircraft ascent in-cloud winds is believed to be somewhat exaggerated due to the large variability in leg-averaged subcloud layer winds as well as the differing methods of determining the winds. Shear is expected to be important near cloud-base, however, as emphasized later in the isentropic analysis and the turbulent kinetic energy budget (section 6). The low level winds obtained from the aircraft transect near C (Fig. 7) further emphasize the acceleration and the changing direction of the wind with time in the boundary layer in the vicinity of the developing cyclone. Moderate low level northerly flow at D contrasts the strong westerly flow at C.

Figure 9 gives a better indication of the horizontal and vertical wind flow near the offshore cyclone. Shown are the winds along isentropic surfaces (constant Θ) obtained from aircraft, ship and CLASS data from 21–22Z on 24 February. Large scale flow in the absence of strong diabatic heating should be roughly along constant Θ surfaces. Such a restriction is satisfied on 24 February provided the profiles over the Gulf Stream (C) and in cloud are not used. At B and D heat fluxes are small (see section 5) and the boundary layer is relatively cloud free. The only clouds in the observation area at this time on 24 February are in association with the cyclone and occur to the east roughly along the western edge of the Gulf Stream. Thus isentropic analysis is not performed at stack C. Even without isentropic analysis over the stratocumulus-topped Gulf Stream MABL, the initial strong cyclonic flow is already evident in Fig. 9 in the clear MABL as far west as stack D about 130 km west-southwest of the cyclone center (L). The 288 K isotherm at a height of roughly 310 m shows cyclonic curvature from D to near the Gulf Stream. From the profiles at B and E, low level flow (40 m) north and east of D exhibits the strong onshore flow evident in the mesoscale analysis (Fig. 3). This confluent/diffluent banding offshore parallel to the East Coast near North and South Carolina, with the diffluent zone approximately 50–70 km offshore over the cold shelf waters (B–D) and the confluent zone further offshore near the western edge of the Gulf

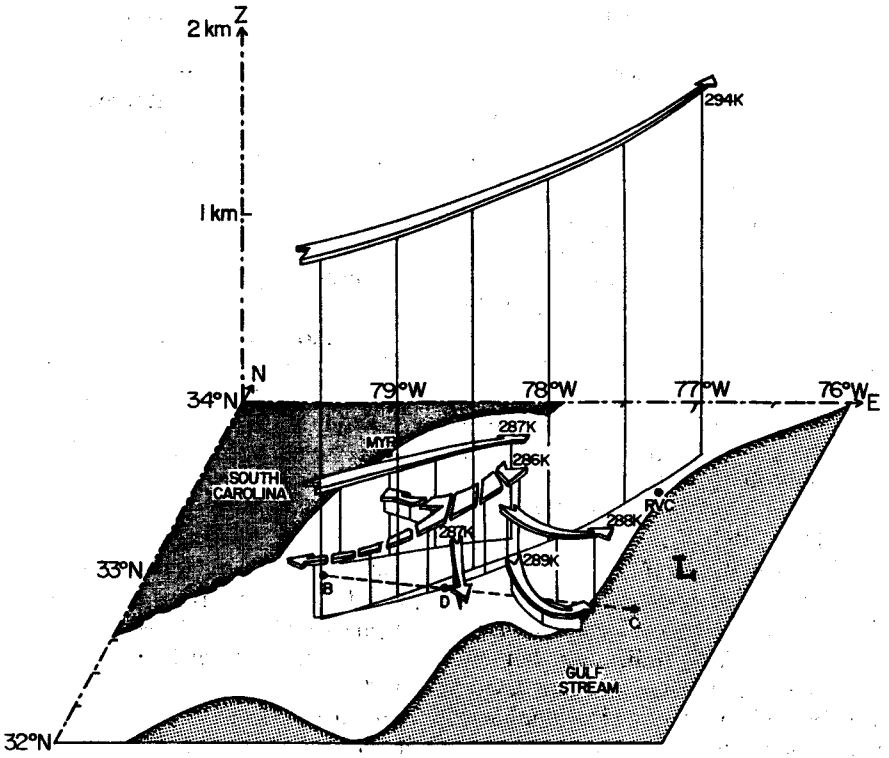

FIG. 9. Schematic of the observation area at 2100 UTC on 24 February in the region of the offshore cyclone. Given are winds along constant Θ surfaces obtained from aircraft, ship and CLASS data. The approximate location of the surface cyclone center is given by L.

Stream was also observed by Riordan (1990) and modeled in a two-dimensional numerical study for onshore flow by Huang and Raman (1988).

Above the near-surface divergent flow pattern between B and D roughly parallel to the coastline, west-southwesterly flow associated with the cyclone is evident at altitudes as low as 500–700 m (Θ = 287 K). This flow accelerates towards the Gulf Stream and thus towards the cyclone center. Estimates of low level divergence from aircraft, buoy and available ship data centered near the western Gulf Stream boundary (C) and near the midshelf front (between B and D) at 2100 UTC 24 February emphasize the differing low level flow patterns. Estimates for the region centered near the midshelf front are obtained from data over a 60 $\times$ 80 km area and indicate a divergence of approximately 6.7×10^{-5} s^{-1}. Estimates near the Gulf Stream are centered at the western boundary over a 50 $\times$ 60 km area with C the easternmost point. Divergent flow is still present (3.3×10^{-5} s^{-1}) but has weakened. This region is west of the cyclone center in an area of strengthening west-southwesterly (W-SW) flow (Fig. 9). Stronger W-SW flow out of the region than weaker northwest flow into the region could explain the divergence. Further east toward the stronger cyclonic rotation, the flow becomes more convergent. Estimates of this convergence are limited by the lack of sufficient data east of the Gulf Stream.

The flow at altitudes between the broad southwesterly flow aloft associated with the free atmosphere and the shallow cyclonic flow near the Gulf Stream emphasize a region of large wind shear above the subcloud layer. Thus, a region of complex wind flow with tremendous horizontal and vertical wind shear is observed offshore in the region of redevelopment of the cyclone. Convergence and consequent acceleration of the wind near the western edge of the Gulf Stream were also observed during GALE for cold air outbreaks (Wayland and Raman 1989). Numerical model studies (Huang and Raman 1988) indicate this to be due to a sea breeze type of circulation superimposed on the mean flow; however, these are the first observations supporting the general hypothesis that the surface baroclinicity is one of the main processes of East Coast cyclogenesis. Zemba and Friehe (1987) similarly found low level baroclinicity important but in the stable MABL in the upwelling regions off the California coast.

5. Turbulence structure

Table 1 shows the MABL parameters for the stacks over the Gulf Stream (stack C) and the midshelf front

TABLE 1. Marine boundary layer parameters over the Gulf Stream (C) and midshelf front region (D).

	24 February	
Region	C	D
Time (UTC)	2057–2139	2205–2245
h (m)	1140	755
w_* (m s^{-1})	1.50	0.86
u_* (m s^{-1})	0.59	0.18
θ_* (K)	0.047	0.029
q_* (g m^{-3})	0.050	0.019
$(\overline{w\theta_v})_0$ (m s^{-1} K)	0.088	0.025
$-L$ (m)	174	17
$-h/L$	6.6	44.4
H (W m^{-2})	87	30
E (W m^{-2})	186	39
Bowen ratio	0.47	0.77

region (stack D) on 24 February. Friction velocity (u_*) is obtained from linear extrapolation to the surface of alongwind and crosswind momentum fluxes at the two lowest flight levels (about 40 and 90 m). Mixed layer scaling parameters of velocity (w_*), temperature (θ_*) and humidity (q_*) are calculated as

$$w_* = [(g/\Theta_v)(\overline{w\theta_v})_0 h]^{1/3}$$
$$\theta_* = (\overline{w\theta})_0 / w_*$$
$$q_* = (\overline{wq})_0 / w_* \quad (1)$$

where $(\overline{w\theta_v})_0$, $(\overline{w\theta})_0$ and $(\overline{wq})_0$ are surface fluxes of virtual potential temperature, potential temperature and absolute humidity, respectively. They are also obtained by linear extrapolation to the surface. The Monin–Obukhov length L is calculated as

$$L = -u_*^3 \Theta_v / [kg(\overline{w\theta_v})_0] \quad (2)$$

where k is von Kármán's constant (0.4).

Also given in Table 1 are surface sensible (H) and latent (E) heat fluxes and the Bowen ratio (equal to H/E):

$$H = \rho c_p (\overline{w\theta})_0$$
$$E = L_v (\overline{wq})_0 \quad (3)$$

where ρ is density, c_p is specific heat of air (1004 J kg^{-1} K^{-1}) and L_v is the latent heat of vaporization.

Due primarily to the effects of the warmer Gulf Stream waters, total heat flux (sensible plus latent) increases dramatically from the midshelf region (D) to the Gulf Stream (C). Figure 10 shows the spatial distribution of total heat flux in the region of the offshore cyclone redevelopment at 2100 UTC 24 February based on aircraft and available ship observations. Fluxes from ship data are calculated by the bulk aerodynamic method (Friehe and Schmitt 1976) with drag coefficient a function of wind speed. The local maximum of total heat flux occurs over the Gulf Stream near C with a strong gradient at the western Gulf Stream boundary (GS). The heat flux gradient weakens

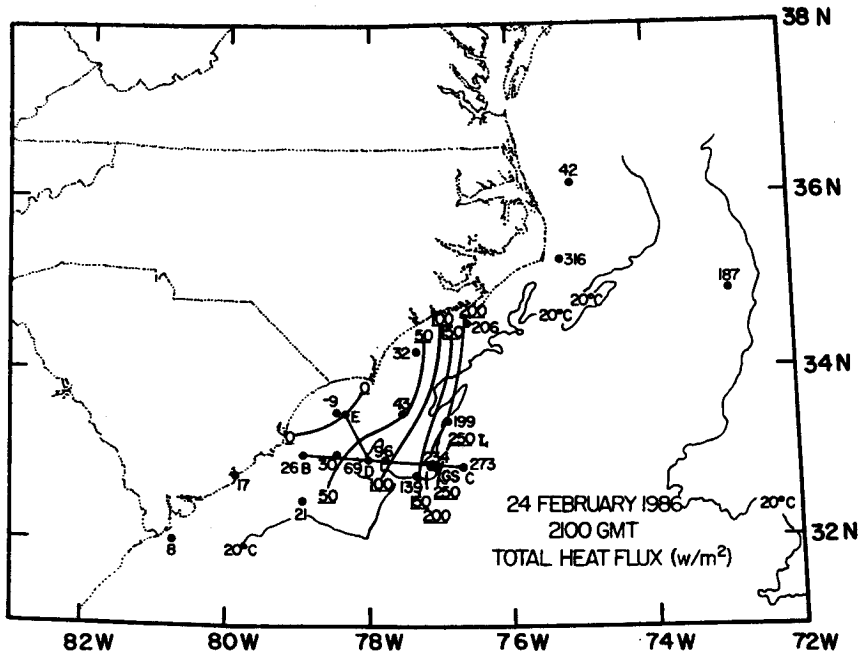

FIG. 10. Horizontal field of total near-surface heat flux obtained from the bulk aerodynamic methods for 2100 UTC on 24 February. Data are from available ship and King Air aircraft observations.

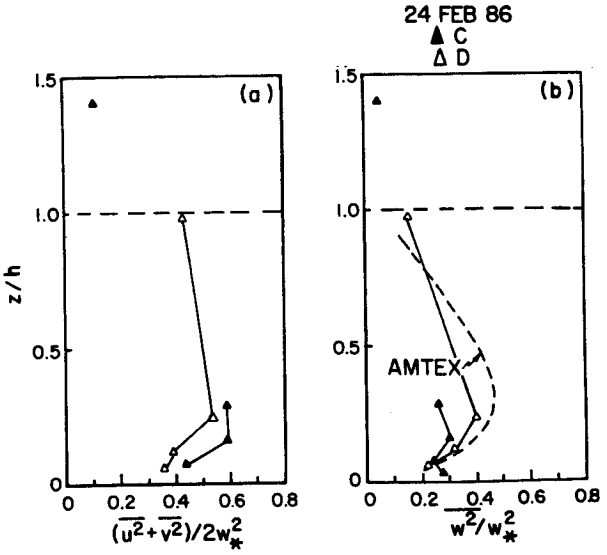

FIG. 11. Normalized (a) horizontal and (b) vertical velocity variances for stacks C and D on 24 February. The value of normalized horizontal velocity variance at C at $z/h = 0.035$ (3.12) is not shown. AMTEX curve is from Lenschow et al. (1980).

considerably westward over the colder shelf waters where the divergent flow is present.

a. Variances

Figure 11 shows the average of the horizontal velocity variances $[(\overline{u^2} + \overline{v^2})/2]$ normalized by w_*^2 along with the normalized vertical velocity variance obtained from King Air stacks at C and D. Horizontal variances at both C and D show a range from 0.4 to 0.6 in the lowest third of the MABL with values generally increasing slightly with height. For stack C this region represents the subcloud layer ($z = 0.32$ h), while for stack D there were no clouds. The range of values shows general agreement with data from other MABL experiments under differing synoptic conditions, such as the Air Mass Transformation Experiment (AMTEX) (Lenschow et al. 1980) and GALE (Grossman and Betts 1990) cases investigating wintertime cold air outbreaks as well as the fair weather trade-wind boundary layer (Pennell and LeMone 1974). The exception is the value of horizontal variance (3.12) at the lowest aircraft level ($z/h = 0.035$) at stack C on 24 February (not shown). This value, larger than those typically observed for MABL's, is believed to be due to a combination of increased low level turbulence caused by both the Gulf Stream and the development of the cyclone.

The normalized vertical velocity variances $\overline{w^2}/w_*^2$, also shown in Fig. 11, are compared to the best fit curve derived from AMTEX measurements characterized as a mesoscale convective (MCC) regime with stability conditions ($-h/L \sim 26$) similar to that at stack D. Data at D agree well with the AMTEX results. At stack C, $\overline{w^2}/w_*^2$ shows a slight overall decrease with height similar to that observed by Brost et al. (1982b) for a shallow stratocumulus-topped MABL. This profile contrasts that of other convective boundary layers (Lenschow et al. 1980) which predict a maximum near $z = 0.3$ h.

The normalized variances of potential temperature and absolute humidity are given in Fig. 12 along with the local free convection curve of Wyngaard et al. (1971). Temperature variances at D are faily well organized and are a closer approximation to the free con-

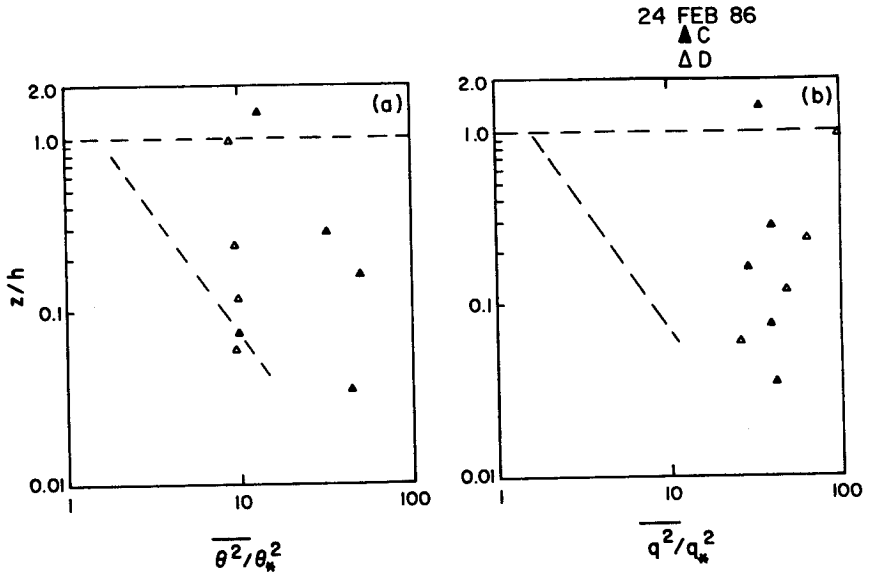

FIG. 12. Normalized potential temperature and humidity variances as in Fig. 11. Dashed diagonal lines are free-convection predictions from Wyngaard et al. (1971).

vection curve than that at stack C. Values at C are much larger than those observed for a convective MABL. The normalized humidity variances q^2/q_*^2 at both stacks are more organized than the temperature variances, showing approximately constant values with height, but are also much larger than free convection predictions.

b. *Fluxes*

The mean momentum budget in the boundary layer can be expressed as

$$\frac{\partial U}{\partial t} + U\frac{\partial U}{\partial x} + V\frac{\partial U}{\partial y} = f(V - V_g) - \frac{\partial}{\partial z}(\overline{uw})$$

$$\frac{\partial V}{\partial t} + U\frac{\partial V}{\partial x} + V\frac{\partial V}{\partial y} = -f(U - U_g) - \frac{\partial}{\partial z}(\overline{vw}) \quad (4)$$

where local time changes and horizontal advection on the left-hand side are balanced on the right-hand side (rhs) by geostrophic departure and friction, respectively. For the budget in this case, a right-handed coordinate system is considered with mean boundary layer wind U aligned with the x-axis. The mean MABL wind direction is taken as 270° for C and 360° for D. Thus, positive U indicates westerly winds for stack C and northerly for D.

Alongwind (U_g) and crosswind (V_g) components of the near-surface (40 m) geostrophic wind are computed from:

$$U_g = -\frac{1}{f\rho}\frac{\partial p}{\partial y}$$

$$V_g = \frac{1}{f\rho}\frac{\partial p}{\partial x} \quad (5)$$

where horizontal pressure gradients are estimated from lowest level aircraft legs and transects in the vicinity of C and D. In the north–south (N–S) direction the gradient is calculated over a distance of roughly 25 km (length of flight leg) and in the east–west (E–W) direction over 85 km (from low level C to D transect). Geostrophic wind shear is obtained from the thermal wind relations

$$\frac{\partial U_g}{\partial z} = -\frac{g}{fT}\frac{\partial T}{\partial y}$$

$$\frac{\partial V_g}{\partial z} = \frac{g}{fT}\frac{\partial T}{\partial x} \quad (6)$$

where horizontal temperature gradients in the N–S direction are calculated over the length of each flight leg. E–W gradients are available only from transect data at 40 and 330 m in the subcloud layer. Thus, E–W gradients at intermediate levels from 40 to 330 m are obtained from linear interpolation of the gradients at 40 and 330 m.

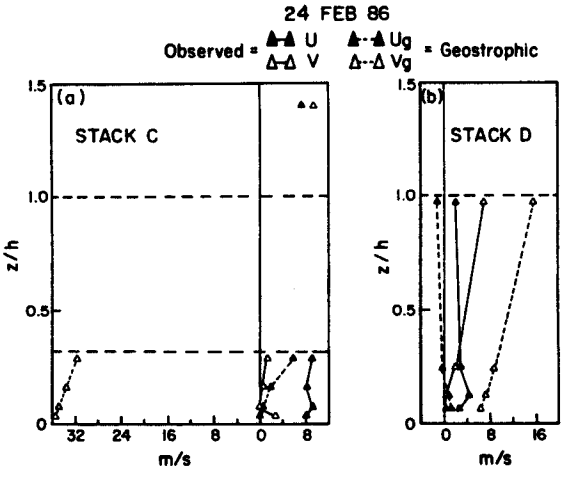

FIG. 13. Vertical profiles of alongwind and crosswind components of observed wind (U, V) and geostrophic wind (U_g, V_g) for (a) stack C and (b) stack D. The dashed horizontal line at $z = 0.32$ h indicates the approximate location of cloud base for stack C.

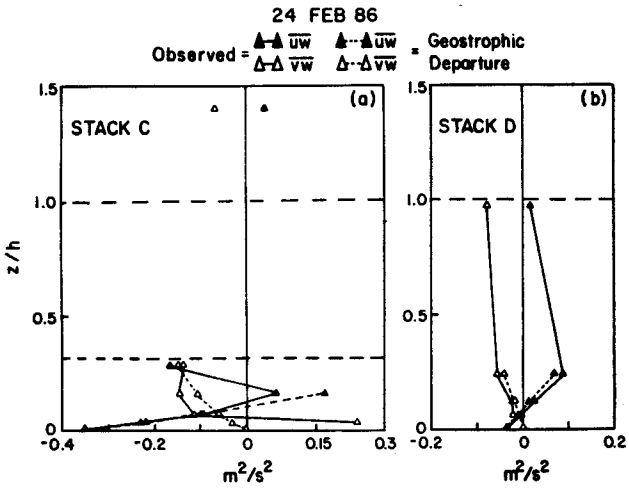

FIG. 14. Alongwind ($\overline{uw}$) and crosswind ($\overline{vw}$) momentum flux profiles for (a) stack C and (b) stack D on 24 February. Solid lines indicate observations obtained from King Air stack data while dashed lines are obtained from the geostrophic departure method. (See text.)

Figure 13 shows the vertical profiles of alongwind and crosswind velocities and Fig. 14 gives the alongwind and crosswind momentum flux or wind stress profiles for stacks C and D. Included in Fig. 14 are flux profiles obtained by integrating the geostrophic departure profiles of Fig. 13. In this integration, the left-hand side of (4) is assumed zero (negligible advection and time changes). Geostrophic departure profiles above $z/h = 0.25$ at D (Fig. 14b) are not included because of the uncertainty in the vertical variation of wind and horizontal temperature gradients over the large distance from $z/h = 0.25$ to 1.0.

The observed momentum flux profiles (solid lines) show curvature consistent with that of a convective, baroclinic boundary layer (Arya and Wyngaard 1975).

The magnitude of momentum fluxes at D is much smaller than that at C, particularly $\overline{uw}$. However, the profiles obtained from geostrophic departure (dashed lines) approximate the alongwind and crosswind stress profiles reasonably well given the approximate nature of the horizontal gradients. Thus, the geostrophic wind and the assumption of negligible advection appear reasonable in this region. The agreement between geostrophic departure and observations at C (Fig. 14a) is not as good with differences evident in the alongwind stress $\overline{uw}$ above $z = 0.2$ h to cloud base ($z = 0.32$ h) and the crosswind stress $\overline{vw}$ near the surface.

The alongwind stress profile at C obtained from geostrophic departure is shown only to a height of approximately $z = 0.2$ h. Above this height the profile is roughly a linear extrapolation to cloud base because of the assumption of a linear variation with height of horizontal temperature gradient $\partial T/\partial x$—resulting in a value of $\overline{uw}$ predicted by geostrophic departure near cloud base much larger than observed. The observed vertical profile of $\overline{uw}$ at C indicates a negative slope above $z = 0.2$ h with $\overline{uw} = -0.17$ m^2 s^{-2} at $z = 0.3$ h. Two possible reasons exist for the large difference between the observed $\overline{uw}$ profile and that predicted by geostrophic departure above $z = 0.2$ h. One is that the assumption of a linear vertical variation of $\partial T/\partial x$ may be false and hence the estimate of the geostrophic wind is in error. Near the surface the linear variation appears valid. Although the magnitude of V_g in the subcloud layer at C (Fig. 13a) is large (-35 m s^{-1}), the geostrophic departure profile closely approximates the observed $\overline{uw}$ profile. Horizontal pressure gradient $\partial p/\partial x$ obtained from low level aircraft transect data from C to D used in calculating V_g near the surface is weak near D but increases dramatically (-3.41×10^{-3} Pa m^{-1}) near C in association with the offshore cyclone. A more probable error in V_g could be the vertical shear near cloud base due to the assumption of a linear vertical variation of $\partial T/\partial x$. Based on this assumption, $V_g = -31$ m s^{-1} at cloud base (Fig. 13). Assuming U_g to be correct, geostrophic wind near cloud base would then be 31.6 m s^{-1} at 349° as compared to approximately 10–12 m s^{-1} at about 240° obtained from the observed wind (Fig. 8). In contrast the estimated geostrophic wind at D near $z = h$ appears more reasonable (15.7 m s^{-1} at 266°) as compared to an observed wind above the boundary layer of 14 m s^{-1} at 255°.

The second explanation for the large difference in the alongwind stress at stack C obtained from geostrophic departure is the neglect of time changes and horizontal advection in the mean momentum budget. Time changes appear negligible over the time period of the King Air flight based on data from ascent and descent profiles at C, but horizontal advection is more difficult to estimate because advection calculations from aircraft data are known to be somewhat unreliable due to averaging time limitations (Lenschow et al. 1980). To balance the momentum budget above $z = 0.2$ h to cloud base, since the wind at C is westerly, $U\partial U/\partial x$ and $U\partial V/\partial x$ must equal 4.2×10^{-3} and -3.0×10^{-4} m s^{-2} respectively. For $U = 10$ m s^{-1}, 1 m s^{-1} changes in U and V over distances of 2.4 and 33 km would be required. For the mesoscale flow evident near the developing cyclone, these distances appear small, although not totally unrealistic. Such changes have been observed across the Gulf Stream boundary (Wayland and Raman 1989; Huang and Raman 1988). Therefore, the neglect of horizontal advection near the Gulf Stream could contribute to the imbalance in the mean momentum budget at C.

Normalized heat and humidity fluxes for stacks C and D are given in Fig. 15. Fluxes at stack C (Fig. 15a, b) emphasize the importance of humidity flux in supplying moisture to the overlying stratocumulus cloud layer. Heat fluxes at C show a near-linear decrease in the subcloud layer with a negative flux near cloud base of approximately -8 W m^2, indicating an overall warming of the subcloud layer as expected. Humidity fluxes at C show a profile similar to the solid or broken stratocumulus cloud cases of Albrecht et al. (1985) in which nearly constant or slightly positive gradients of $\overline{wq}$ with height in the subcloud layer indicated small overall moistening of the cloud layer and subsequent drying of the subcloud layer. In contrast to Albrecht et al. (1985), however, the vertical gradient of $\overline{wq}$ up to approximately $z = 0.2$ h does indicate a moistening of the subcloud layer as expected for decreasing cloud base over the Gulf Stream region while the magnitude of the humidity flux at C is also 4 to 8 times that of Albrecht et al. (1985). The magnitude of humidity fluxes at C (approximately 180–200 W m^{-2}) dominates sensible heat flux indicating the importance of the Gulf Stream in supplying moisture to the stratocumulus-topped MABL at C.

The flux profiles at D in the clear MABL (Figs. 15c, d) show a vertical structure more typical of a convective, largely cloud-free MABL. Heat fluxes decrease nearly linearly with height with a value of approximately -0.24 at $z = h$, in agreement with previous observational and theoretical values ranging from -0.1 to -0.3 (Stull 1976). Humidity fluxes at D show an increase with height near the surface up to approximately $z = 0.25$ h but little flux near $z = h$ for the clear MABL.

6. Turbulent kinetic energy (TKE) budget

Assuming horizontal homogeneity, the TKE budget in the MABL can be expressed as

$$\frac{\partial \bar{e}}{\partial t} = -\overline{uw}\frac{\partial U}{\partial z} - \overline{vw}\frac{\partial V}{\partial z} + \frac{g}{\Theta_v}\overline{w\theta_v} - \frac{\partial}{\partial z}(\overline{we}) - \frac{1}{\rho}\frac{\partial}{\partial z}(\overline{wp}) - \epsilon \quad (8)$$

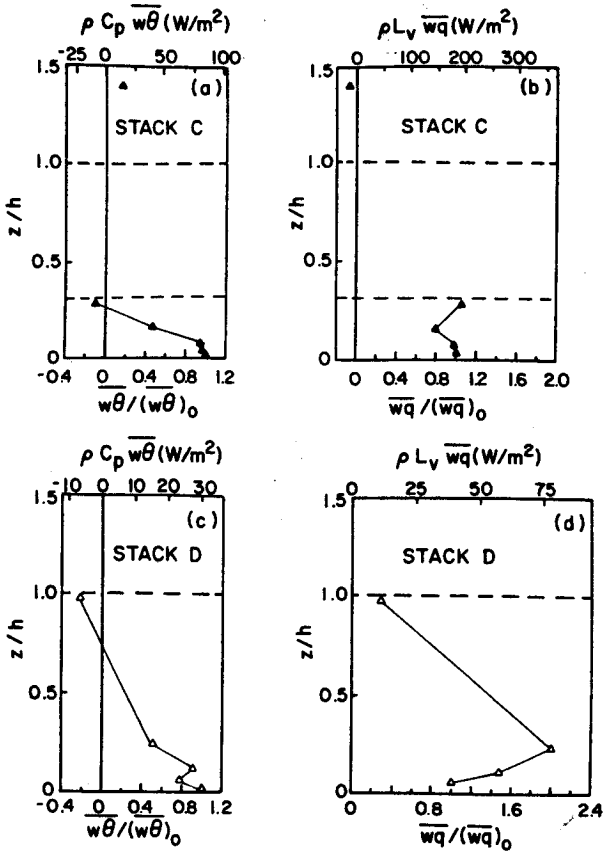

FIG. 15. Normalized heat and moisture fluxes at stacks C and D on 24 February. The upper abscissa also give approximate values of sensible and latent heat fluxes (W m^{-2}).

where turbulent kinetic energy $e = 0.5(u^2 + v^2 + w^2)$, and p is fluctuating pressure. The first two terms on the rhs of (8) are alongwind and crosswind shear production (S), the third term is buoyancy production (B), the fourth is turbulent transport (T), the fifth is pressure transport (P) and the sixth is viscous dissipation. The TKE budget can then be expressed as

$$S + B + T + P + \epsilon = I \qquad (9)$$

where the imbalance (I) is the term required to balance the TKE budget and includes horizontal and vertical advection, temporal changes and any measurement errors.

In the determination of shear production, vertical gradients of alongwind or crosswind velocity are calculated by simple finite difference of two stack legs. Accordingly, momentum fluxes are then taken as the average of the two legs. Turbulent transport (T) is obtained from finite differencing of the turbulence energy flux $\overline{we}$ shown in Fig. 16a. The normalized data in the lowest third of the MABL at stack D are fit well by

$$\overline{we}/w_*^3 = 0.45(z/h)(1 - 0.9z/h)^2 \qquad (10)$$

which is roughly half that of AMTEX (Lenschow et al. 1980) and one-third that of MASEX (Chou et al. 1986) for cold air outbreaks. Values of $\overline{we}/w_*^3$ at C (over the Gulf Stream), particularly near the surface and cloud base, do not appear to follow the normalized curves as given for stack D or other MABL experiments. The large value near the surface, indicating more effective eddy transport of TKE as compared to D, is probably influenced by both the Gulf Stream and the low level cyclone.

Profiles of the normalized vertical flux of TKE divided between horizontal and vertical variances are shown in Figs. 16b and 16c. The normalized vertical flux of vertical velocity variance $0.5\overline{w^3}/w_*^3$ for both stacks C and D is approximated in the lowest third of the MABL by

$$\overline{w^3}/w_*^3 = 0.32(z/h)(1 - 0.8z/h)^2 \qquad (11)$$

which is approximately half that of AMTEX and one-seventh that of MASEX.

The ratio of the vertical fluxes of horizontal and vertical velocity variance $[\overline{w(u^2 + v^2)}/\overline{w^3}]$ (as can be inferred from Fig. 16) at D agrees well with both AMTEX and MASEX data and also the model proposed by Lenschow (1974). The ratio is slightly greater than 1 in the surface layer but less than 1 throughout the MABL showing a slightly larger contribution of vertical velocity variance to turbulent transport. In the subcloud layer at stack C (Gulf Stream), however, the flux of horizontal velocity variance is as much as five times larger than that of vertical velocity variance. Closer to the surface the dominance of $\overline{w(u^2 + v^2)}$ (more than 20 times that of $\overline{w^3}$) is believed to be due to the increased shear generation and turbulence in u and v associated with the developing cyclone. Brost et al. (1982) also found the flux of horizontal variance to dominate turbulent transport for the marine stratocumulus boundary layer off the California coast; however, their increase was not associated with a developing cyclone.

Pressure transport P is not measured but is obtained from (Zeman and Lumley 1976):

$$P = -\frac{1}{\rho}\frac{\partial}{\partial z}(\overline{wp}) = 0.4\frac{\partial}{\partial z}(\overline{we}) \qquad (12)$$

such that pressure transport cancels 40% of turbulent transport. Viscous dissipaton ϵ was obtained from the inertial subrange of the vertical velocity spectra:

$$S_w(f) = 0.67(U_a/2\pi)^{2/3}\epsilon^{2/3}f^{-5/3} \qquad (13)$$

where f is frequency (range of 5–10 Hz for inertial subrange), $S_w(f)$ is the vertical velocity spectra and U_a is the aircraft speed (80 m s^{-1}).

The TKE budget on 24 February at stacks C and D normalized by w_*^3/h is given in Fig. 17. The budget at C, calculated only for the subcloud layer, is dominated by dissipation and near-surface shear production.

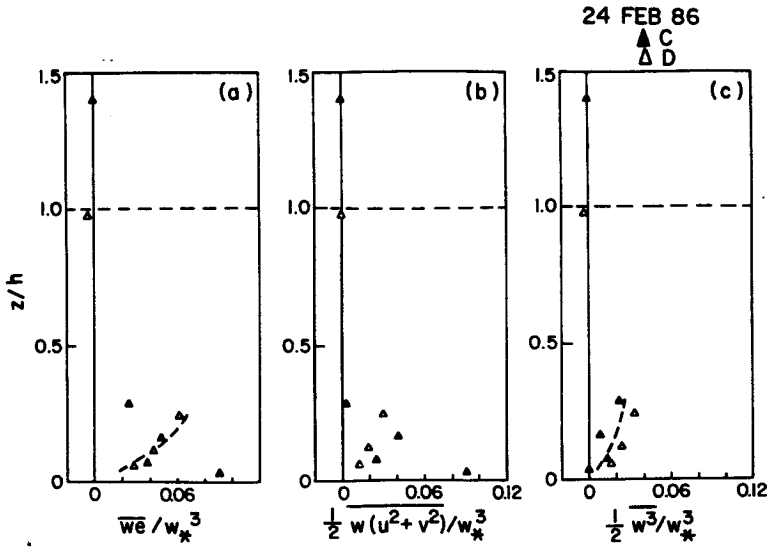

FIG. 16. Vertical profiles of normalized (a) turbulence energy flux, (b) vertical flux of horizontal variance and (c) vertical flux of vertical variance for stacks C and D. Dotted lines are best fit curves to the data in the subcloud layer. (See text.)

Buoyancy is relatively unimportant in the lowest third of the subcloud layer. To balance the large shear production, normalized dissipation near the surface is much larger than observed for other subcloud layer TKE budgets such as Brost et al. (1982b) or Zemba and Friehe (1987). Turbulent transport T is also larger near the surface. The dashed line of T near the surface shown in Fig. 17a is calculated assuming $\overline{we} = 0$ at the surface and also that $\overline{we}$ at the lowest level (0.307 m^3 s^{-3} at $z/h = 0.035$) is correct. Such an assumption gives large normalized turbulent transport ($T = -3.46$) out of the lower MABL but also a shallow region of downward transport from $z/h = 0.05$ to 0.12. Based on the small magnitude of the imbalance (I) near the surface, however, it appears that large transport is necessary to help balance the large shear generation.

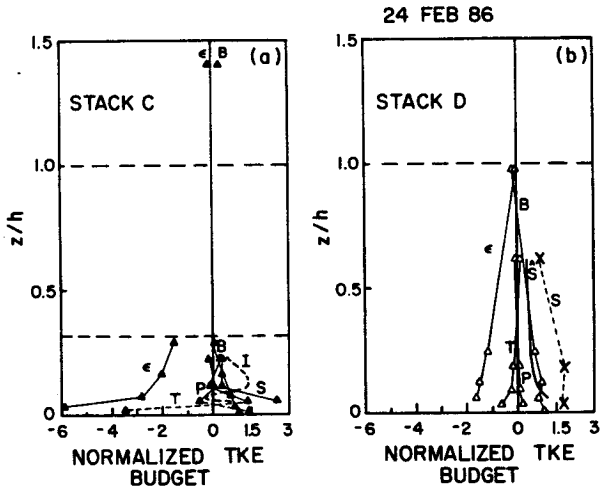

FIG. 17. Vertical profiles of the TKE budgets for (a) stack C and (b) stack D on 24 February 1986 normalized by $w_*^3 h^{-1}$. Curves are given for shear production (S), buoyancy production (B), turbulent transport (T), pressure transport (P), dissipation (ϵ) and the imbalance (I). For stack D, shear values obtained from King Air stack data are given as (x), while curve S is the imbalance of B, ϵ, P and T. The near-surface value of shear (S) for stack C is not shown but is approximately 23.5.

In the upper third of the subcloud layer at C, shear and buoyancy production are roughly equal but the imbalance indicates a deficit in TKE production aloft. It is possible that dissipation (ϵ) near cloud base is overestimated due to the lack of an inertial subrange in the measured velocity spectra (Chou et al. 1986). Dissipation does show a typical profile in the MABL with a rapid decrease near the surface approaching a near-constant value in the middle of the subcloud layer; however, dissipation (ϵ) is still a large sink term in the TKE budget near cloud base. Large shear production near cloud base could provide the production term necessary to balance the budget (see Fig. 8). Pressure transport, known to act with turbulent transport near cloud base (Deardorff 1980), would also help reduce the imbalance.

The TKE budget at D is shown in Fig. 17b. Curves are the same as in Fig. 17a with the exception of S and I. Given are the values of shear production (S) calculated from aircraft leg-averaged values (x) as at C. These values are of less certainty than shear production at C. With weak winds on the order of 2–4 m s^{-1} and standard deviations of 0.5 to 0.7 m s^{-1}, vertical shear is more difficult to accurately estimate. The smaller stress profiles at D (Fig. 14) are also more subject to error than at C. Instead of the calculated values of shear production, curve S in Fig. 17b represents the imbalance of B, ϵ, P and T. This curve appears more rea-

sonable than the calculated values of shear production at D where S is expected to be insignificant in the boundary layer ($-L \ll h$).

Comparison of the two TKE budgets indicate significant differences. The most obvious difference is the large magnitude of all normalized terms at C. Thus for a given heat flux, the MABL processes at C over the Gulf Stream and closer to the developing low level cyclone are much more active in producing, dissipating and transferring TKE. Shear is the dominant production term at C in the subcloud layer, but buoyancy and even turbulent transport contribute to TKE for levels below $z/h = 0.2$. At D, shear and buoyancy are TKE sources but of much less magnitude than at C. Normalized turbulent transport at D is likewise much smaller than at C.

Based on the stability parameter $-h/L$, normalized TKE budgets at C and D compare favorably with those of other MABLs. Compared to budgets of AMTEX (Lenschow et al. 1980) and that of Lenschow (1974) with similar $-h/L$, buoyancy and turbulent transport profiles are approximately equal to those at D on 24 February. Dissipation at stack D is approximately twice that of AMTEX as is shear production (S). The TKE budget at C with $-h/L = 6.6$ agrees reasonably well with the 13 June budget of Brost et al. (1982) for a marine stratocumulus-topped boundary layer with similar MABL characteristics ($-h/L = 1.35$). Each budget is dominated by shear and dissipation with buoyancy insignificant in the lower MABL, but normalized shear and dissipation at C are larger in magnitude near the surface. A major difference in the budgets is the importance of turbulent transport at C. Normalized transport for Brost et al. (1982) is approximately -0.5 up to $z/h = 0.4$ compared to -3.5 at $z/h = 0.035$ at C. Compared to the MASEX TKE budget (Chou et al. 1986) with $-h/L = 13$, normalized shear production and dissipation at C on 24 February are three to four times larger.

7. Conclusions

Marine boundary layer structure and circulation in the vicinity of offshore redevelopment and intensification of an onshore surface cyclone are documented from GALE data on 24 February 1986. Results emphasize the differing nature of the marine boundary layer affected by the development of an offshore cyclone as compared to typically observed quasi-stationary cold air outbreak MABLs or over-land convective boundary layers. Data obtained from over the cold shelf waters (B), midshelf front (D) and the Gulf Stream (C) separated by about 200 km emphasize the markedly different nature of the boundary layers. Mean structure at D shows a near-neutral MABL with very light and variable winds. This is a cloud-free region, as seen from satellite pictures, characterized by large scale divergence and diffluence. Mesoscale analysis of ship, aircraft and PAM data indicate a broad zone of diffluent flow in the wind field approximately 50–70 km offshore aligned along the cold shelf waters. In addition, estimates of low level divergence near the midshelf front (D) are on the order of 7×10^{-5} s^{-1} compared to weaker divergence eastward approaching the Gulf Stream and convergence across the western edge of the Gulf Stream in the vicinity of the developing cyclone.

In contrast, mean structure at C over the Gulf Stream shows a MABL topped by layered stratocumulus with a low inversion base (360 m), strong, unidirectional winds, near-neutral stability and relatively thick (800–1200 m) cloud layer. While investigating the differences between the mean structure at C and other stratocumulus-topped MABLs, however, the implications of the larger synoptic-scale cyclonic motion must be considered. Satellite information from 2000–2200 UTC (Fig. 4) indicated that the cyclone was developing about 50 km north-northeast of C at the time of aircraft observations. This provided a unique opportunity to examine the effects of cyclone redevelopment on MABL structure and vice versa.

Imbedded beneath the broad southwesterly flow aloft on 24 February is a complex mesoscale flow in association with the offshore movement of the cyclone. Strong low level cyclonic flow is observed about the shallow warm dome situated near the Gulf Stream.

Flux profiles agree with results from MABLs under similar cloud and stability conditions. Subcloud layer warming and moistening is evident at stack C over the Gulf Stream from low level heat and moisture flux convergence. Consequently the depth of the subcloud layer decreases from near the western edge of the Gulf Stream eastward to stack C while the depth of the cloud layer increases as typically observed for offshore fetches during cold air outbreaks (Grossman and Betts 1990; Wayland and Raman 1989). Moisture flux is found to dominate heat flux in the subcloud layer over the Gulf Stream while the fluxes in the clear midshelf front MABL are approximately four times smaller.

Comparison of turbulent kinetic energy (TKE) budgets over the Gulf Stream (stack C) and the midshelf front (stack D) emphasize the differences in MABL processes. In the subcloud layer at C with strong winds and $-h/L = 6.6$, shear production and dissipation dominate as was observed by Brost et al. (1982); however, at C turbulent transport is also a significant sink term in the TKE budget near the surface. The budget at D with light winds and weak buoyancy and momentum fluxes is similar to that of AMTEX (Lenschow et al. 1980). Shear production at D is less significant in the middle of the MABL than at C, and all normalized TKE terms are of smaller magnitude than observed at C indicating a much less active boundary layer for a given heat flux.

Temperature and moisture turbulence structure over both the midshelf front and the Gulf Stream is less well organized than the flux profiles. Low level horizontal

and vertical velocity variances at C and D show general agreement with corresponding clear and stratocumulus-topped MABLs. Friction velocity is 3 times larger at C. In the TKE budget normalized shear production at C is 23 times larger in the surface layer than buoyancy. Turbulent transport at C is a significant term due primarily to the flux of horizontal velocity variance, which is five times that of the flux of vertical velocity variance. Thus, the most obvious effects of the offshore redevelopment and intensification of the cyclone on MABL structure are seen in the mean and turbulence wind structure.

Acknowledgments. This work was supported by the National Science Foundation Division of Atmospheric Sciences under Grants ATM-83-11812 and ATM-88-01650.

REFERENCES

Albrecht, B. A., R. S. Penc and W. H. Schubert, 1985: An observational study of cloud-topped mixed layers. *J. Atmos. Sci.*, **42**, 800–822.

Arya, S. P. S., and J. C. Wyngaard, 1975: Effect of baroclinicity on wind profiles and the geostrophic drag law for the convective planetary boundary layer. *J. Atmos. Sci.*, **32**, 767–778.

Bosart, L. F., and S. C. Lin, 1984: A diagnostic analysis of the Presidents' Day storm of February 1979. *Mon. Wea. Rev.*, **112**, 2148–2177.

Brost, R. A., J. C. Wyngaard and D. H. Lenschow, 1982a: Marine stratocumulus layers. Part I: Mean conditions. *J. Atmos. Sci.*, **39**, 800–817.

——, —— and ——, 1982b: Marine stratocumulus layers. Part II: Turbulence budgets. *J. Atmos. Sci.*, **39**, 818–836.

Brown, E. N., C. A. Friehe and D. H. Lenschow, 1983: The use of pressure fluctuations on the nose of an aircraft for measuring air motion. *J. Climate Appl. Meteor.*, **22**, 171–180.

Chou, S.-H., and J. Zimmerman, 1989: Bivariate conditional sampling of buoyancy flux during an intense cold-air outbreak. *Bound.-Layer Meteor.*, **46**, 93–112.

——, D. Atlas and E.-N. Yeh, 1986: Turbulence in a convective marine atmospheric boundary layer. *J. Atmos. Sci.*, **43**, 547–564.

Deardorff, J. W., 1980: Stratocumulus-capped mixed layers derived from a three-dimensional model. *Bound.-Layer Meteor.*, **18**, 495–527.

Dirks, R. A., J. P. Kuettner and J. A. Moore, 1988: Genesis of Atlantic Lows Experiment (GALE): An overview. *Bull. Amer. Meteor. Soc.*, **69**, 148–160.

Friehe, C. A., and K. F. Schmitt, 1976: Parameterization of air–sea interface fluxes of sensible heat and moisture by the bulk aerodynamic formulas. *J. Phys. Oceanogr.*, **6**, 801–809.

——, R. L. Grossman and Y. Penn, 1986: Calibration of an airborne Lyman-alpha hygrometer and measurement of water vapor flux using a thermoelectric hygrometer. *J. Atmos. Oceanic Technol.*, **3**, 299–304.

Grossman, R. L., and A. K. Betts, 1990: Air–sea interaction during an extreme cold air outbreak from the eastern coast of the United States. *Mon. Wea. Rev.*, **118**, 324–342.

Gyakum, J. R., 1983: On the evolution of the QEII storm. Part II: Dynamic and thermodynamic structure. *Mon. Wea. Rev.*, **111**, 1156–1173.

Huang, C.-Y., and S. Raman, 1988: A numerical modeling study of the marine boundary layer over the Gulf Stream during cold air advection. *Bound.-Layer Meteor.*, **45**, 251–290.

LeMone, M. A., 1973: The structure and dynamics of horizontal roll vortices in the planetary boundary layer. *J. Atmos. Sci.*, **30**, 1077–1091.

——, and W. T. Pennell, 1980: A comparison of turbulence measurements from aircraft. *J. Appl. Meteor.*, **19**, 1420–1437.

Lenschow, D. H., 1974: Model of the height variation of the turbulence kinetic energy budget in the unstable planetary boundary layer. *J. Atmos. Sci.*, **31**, 465–474.

——, J. C. Wyngaard and W. T. Pennell, 1980: Mean-field and second-moment budgets in a baroclinic, convective boundary layer. *J. Atmos. Sci.*, **37**, 1313–1326.

——, and P. Spyers-Duran, 1986: Measurement techniques: Air motion sensing. NCAR Bulletin No. 23. [Available from NCAR, Boulder, CO 80307.]

Mercer, T. J., and C. W. Kreitzberg, 1986: GALE Field Program Summary. [Available from Dept. of Physics and Atmospheric Sci., Drexel University, Philadelphia, PA 19104.]

Nuss, W. A., and R. A. Anthes, 1987: A numerical investigation of low-level processes in rapid cyclogenesis. *Mon. Wea. Rev.*, **115**, 2728–2743.

Pennell, W. T., and M. A. LeMone, 1974: An experimental study of turbulence structure in the fair-weather trade wind boundary layer. *J. Atmos. Sci.*, **31**, 1308–1323.

Raman, S., and A. J. Riordan, 1988: The Genesis of Atlantic Lows Experiment: The Planetary-Boundary-Layer subprogram of GALE. *Bull. Amer. Meteor. Soc.*, **69**, 161–172.

Riordan, A. J., 1990: Examination of the mesoscale features of the GALE coastal front of 24–25 January 1986. *Mon. Wea. Rev.*, **118**, 258–282.

Stull, R. B., 1976: The energetics of entrainment across a density interface. *J. Atmos. Sci.*, **33**, 1260–1267.

Wayland, R. J., and S. Raman, 1989: Mean and turbulent structure of a baroclinic marine boundary layer during the 28 January 1986 cold-air outbreak (GALE86). *Bound.-Layer Meteor.*, **48**, 227–254.

Wyngaard, J. C., O. R. Cote and Y. Izumi, 1971: Local free convection, similarity, and the budgets of shear stress and heat flux. *J. Atmos. Sci.*, **28**, 1171–1182.

Zeman, O., and J. L. Lumley, 1976: Modeling buoyancy driven mixed layers. *J. Atmos. Sci.*, **33**, 1974–1988.

Zemba, J., and C. A. Friehe, 1987: The marine atmospheric boundary layer jet in the Coastal Ocean Dynamics Experiment. *J. Geophys. Res.*, **92**, 1489–1496.